Limits on radioactive powered emission associated with a short-hard GRB 070724A in a star-forming galaxy

Daniel Kocevski,[1]* Christina C. Thöne,[2] Enrico Ramirez-Ruiz,[3] Joshua S. Bloom,[4] Jonathan Granot,[5] Nathaniel R. Butler,[4] Daniel A. Perley,[4] Maryam Modjaz,[4]† William H. Lee,[6] Bethany E. Cobb,[2] Andrew J. Levan,[7] Nial Tanvir[8] and Stefano Covino[2]

[1]*Kavli Institute for Particle Astrophysics and Cosmology, Stanford University, 2575 Sand Hill Road M/S 29, Menlo Park, CA 94025, USA*
[2]*Istituto Nazionale di Astrofisica, Osservatorio Astronomico di Brera,Via E. Bianchi 46, 23807 Merate, Italy*
[3]*Department of Astronomy and Astrophysics, University of California, Santa Cruz, CA 95064, USA*
[4]*Department of Astronomy, University of California, Berkeley, CA 94720-3411, USA*
[5]*Centre for Astrophysics Research, University of Hertfordshire, College Lane, Hatfield, Herts AL10 9AB*
[6]*Instituto de Astronomia, Universidad Nacional Autonoma de Mexico (UNAM), Apdo. Postal 70-264, Cd. Universitaria, Mexico DF 04510, Mexico*
[7]*Department of Physics, University of Warwick, Coventry CV4 7AL*
[8]*Department of Physics and Astronomy, University of Leicester, University Road, Leicester LE1 7RH*

ABSTRACT

We present results of an extensive observing campaign of the short-duration, hard spectrum gamma-ray burst (GRB) 070724A, aimed at detecting the radioactively powered emission that might follow from a binary merger or collapse involving compact objects. Our multiband observations span the range in time over which this so-called Li–Paczyński mini-supernova (mini-SN) could be active, beginning within 3 h of the GRB trigger and represent some of the deepest and most comprehensive searches for such emission. We find no evidence for such activity and place limits on the abundances and the lifetimes of the possible radioactive nuclides that could form in the rapid decompression of nuclear density matter. Furthermore, our limits are significantly fainter than the peak magnitude of any previously detected broad-lined Type Ic SN associated with other GRBs, effectively ruling out a long GRB-like SN for this event. Given the unambiguous redshift of the host galaxy ($z = 0.456$), GRB 070724A represents one of a small, but growing, number of short-hard GRBs for which firm physical/rest-frame quantities currently exist. The host of GRB 070724A is a moderately star-forming galaxy with an older stellar population component and a relatively high metallicity of $12 + \log(O/H)_{KD02} = 9.1$. We find no significant evidence for large amounts of extinction along the line of sight that could mask the presence of an SN explosion and estimate a small probability for chance alignment with the putative host. We discuss how our derived constraints fit into the evolving picture of short-hard GRBs, their potential progenitors and the host environments in which they are thought to be produced.

Key words: gamma-rays: bursts.

1 INTRODUCTION

Long-duration gamma-ray bursts (GRBs), lasting more than ∼2 s (Kouveliotou et al. 1993), are thought to originate from the collapse of massive stars (see Woosley & Bloom 2006). Short-duration, hard spectrum, gamma-ray bursts (SHBs), with a duration of less than ∼2 s have long been assumed to have a different astrophysical origin than long-duration events (Lee & Ramirez-Ruiz 2007; Nakar 2007), namely the coalescence of compact binaries, the most widely discussed being neutron star binaries (NS–NS) or a neutron star and a black hole binary (NS–BH) (Paczynski 1986; Eichler et al. 1989; Narayan, Piran & Shemi 1991; Paczynski 1991). The discovery of afterglows associated with SHBs (Gehrels et al. 2005; Hjorth et al. 2005b) led to the inference that they are associated with an older population of stars (e.g. Bloom et al. 2006). Subsequent follow-up observations supported the idea that these events would

*E-mail: dankocevski@gmail.com
†Miller Fellow.

not be accompanied by SNe (Hjorth et al. 2005b; Bloom et al. 2006).

Nominally, without explosive nucleosynthesis of ^{56}Ni to form an SN, there should be no late-time optical emission after the afterglow has faded. However, during an NS–NS or NS–BH merger, dense material stripped from the star has been predicted to form large tidal tails (Rosswog 2007). Depending on the details of the encounter and the neutron star equation of state, a fraction of this can be dynamically ejected from the system. The subsequent decompression of this material could synthesize radioactive elements through the *r*-process (Freiburghaus, Rosswog & Thielemann 1999; Rosswog et al. 1999), whose radioactive decay could power an optical transient (Li & Paczyński 1998). The fraction of material that remains bound will eventually return to the vicinity of the compact object, with possible interesting consequences for late-time emission (Lee & Ramirez-Ruiz 2007; Rosswog 2007; Lee, Ramirez-Ruiz & López-Cámara 2009).

For a number of SHBs, late-time limits on additional light arising from Type Ib/c SNe, which have been associated with some long GRBs, have been obtained: 050509B (Hjorth et al. 2005a; Bloom et al. 2006), 050709 (Fox et al. 2005; Hjorth et al. 2005a), 050724 (Malesani et al. 2007), 051221A (Soderberg et al. 2006), 050813 (Ferrero et al. 2007), 060502B, where the limits range from 1.5 to over 6 mag fainter than GRB–SN 1998bw. Limits on a mini-SN-like scenario at early times ($\sim$1 d) have so far only been derived for GRB 050509B (Hjorth et al. 2005a; Bloom et al. 2006), setting an upper limit of $\leq 10^{-5}$ on the fraction of rest mass energy that goes into the radioactive decay. Though an optical Li–Paczyński mini-supernova (LP-SN) (Li & Paczyński 1998) like bump was seen in GRB 080503 (Perley et al. 2008), concurrent X-ray emissions suggested a synchrotron-powered afterglow, rather than a radioactive powered event, better accounted for the physical origin. Furthermore, no redshift was available for that event, so the energetics of the additional emission contributing to the 1-d bump are unconstrained.

Here, we report on new LP-SN limits of an SHB. GRB 070724A was detected by the *Swift* satellite on 2007 July 24 10:53:50 UT and consisted of a single peak with a duration of $T_{90} = 0.4 \pm 0.04$ s (Parsons et al. 2007; Ziaeepour et al. 2007). The X-ray telescope (XRT) instrument onboard *Swift* revealed a counterpart 77.8 arcsec from the centre of the Burst Alert Telescope (BAT) position (Page & Ziaeepour 2007; Parsons et al. 2007). Optical afterglow was detected neither by the Ultraviolet/Optical Telescope (UVOT) instrument (de Pasquale & Ziaeepour 2007) nor from ground-based observations (Cenko et al. 2007; Covino et al. 2007). A nearby Digital Sky Survey (DSS) source, 0.5 arcsec from the centre of the XRT position was quickly proposed as a possible host (Bloom 2007; Bloom & Butler 2007) with a redshift of $z = 0.457$ (Cucchiara et al. 2007) and found not to be varying (Covino et al. 2007; Cucchiara et al. 2007). Four radio sources were also found inside the BAT error circle, although none showed any sign of variability (Chandra & Frail 2007). The field containing the host galaxy was visible near the end of the night over most of North America, allowing for comprehensive follow-up observations by a variety of telescopes over the course of several weeks.

The paper is organized as follows. In Section 2, we present a summary of our observations. The results of the mini-SN modelling are presented in Section 3, while the properties of the suggested host galaxy and surrounding galaxy population is discussed in Section 4. Finally, the implications of our results are presented in Section 5. Throughout the paper, we assume $H_0 = 71$ km s^{-1} Mpc^{-1} and a Λ cold dark matter cosmology with $\Omega_m = 0.27$ and $\Omega_\Lambda = 0.73$.
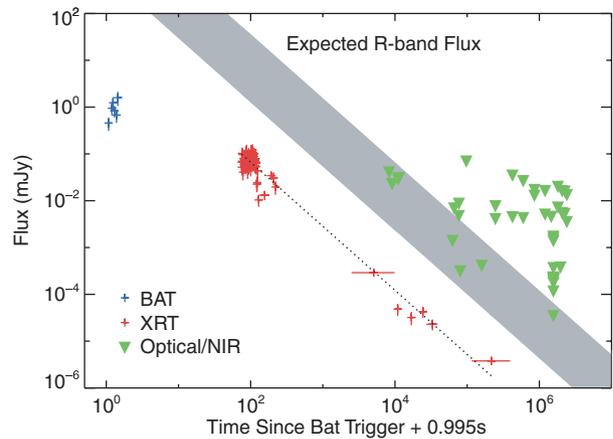

Figure 1. Gamma-ray (blue) and X-ray (red) observations of GRB 070724A along with our optical and NIR (green) upper limits. The grey region represents the expected *R*-band flux from a standard forward shock model given the afterglow's X-ray properties. Our optical observations rule out a bright optical afterglow for this event.

2 OBSERVATIONS AND ANALYSIS

2.1 *Swift* BAT and XRT

The detection of GRB 070724A prompted an automated slew of the *Swift* spacecraft followed by XRT observations of the field beginning at $T + 72.1$ s and which continued for roughly $\sim$10^6 s, at which point the source faded below the detector's sensitivity threshold. We obtained the *Swift* BAT and XRT data on GRB 070724A from the *Swift* archive.[1] The data were processed with version 0.11.4 of the XRTPIPELINE reduction script from the HEASOFT 6.3.1[2] software release, where we have employed the latest (2007-07-09) calibration files at time of writing. The reduction of XRT data from cleaned event lists output by XRTPIPELINE to science-ready light curves and spectra is described in detail in Butler & Kocevski (2007a).

Our best estimate of the position of the XRT detection is $\alpha = 01^h51^m13\overset{s}{.}99$, $\delta = -18°35'39\overset{''}{.}1$ with an error of $\sim$2 arc-sec. The fluence in the 15–150 keV BAT energy band is $3.0 \pm 0.7 \times 10^{-8}$ erg cm^{-2}. This is an extremely low value when compared to other *Swift*-detected GRBs, being among the faintest 2 per cent of *Swift* bursts and the faintest 20 per cent of *Swift*-detected short bursts. Given the redshift $z = 0.457$, reported by Cucchiara et al. (2007), the isotropic equivalent energy released in gamma-rays is estimated at $E_{\mathrm{iso}} = 1.55 \times 10^{49}$ erg.

The XRT light curve (Fig. 1) is consistent with an unbroken power law with a decay index ($F_\nu \propto t^{-\alpha}$) of $\alpha_X = 1.37 \pm 0.03$ over the entire span of the *Swift* observations. The windowed timing mode spectrum from $t = 74$ s to 4.1 ks after the burst is well-fitted by a power law with photon index ($\mathrm{d}N/\mathrm{d}E \propto E^{-\Gamma}$) of $\Gamma = 1.5$ or correspondingly an energy index ($F_\nu \propto \nu^{-\beta}$) of $\beta_X = 0.5$, and photoelectric absorption yielding $N_H = 2.4 \pm 0.9 \times 10^{22}$ cm^{-2}, significantly greater than Galactic ($N_{H,\mathrm{Galactic}} = 1.2 \times 10^{20}$ cm^{-2}; Kalberla et al. 2005).

We note that there are significant and rapid variations at early times in the X-ray hardness, which suggest that the excess column is a spurious result of the simple model assumption and that this emission is not due to the external shock afterglow (cf. Butler &

[1] ftp://legacy.gsfc.nasa.gov/swift/data
[2] http://heasarc.nasa.gov/docs/software/lheasoft/

Kocevski 2007a). Indeed, there are no hardness variations after $t \approx 300$ s, and the excess column density for the photon counting (PC) mode spectrum at these times is $N_{\mathrm{H,excess}} = 0.5(-0.5, +3.5) \times 10^{22}$ cm^{-2} (90 per cent confidence interval), consistent with the Galactic value. The hardness at this time is consistent with the $\Gamma = 2.0$ commonly observed in other XRT-detected GRBs, both long and short. (Butler & Kocevski 2007b).

Assuming $N_{\mathrm{H}} = 1.2 \times 10^{20}$ cm^{-2} and $\Gamma = 2.0$ ($\beta_{\mathrm{X}} = -1.0$), the conversion from the 0.3–10.0 keV count rate to flux in μJy at 1 keV is 0.044 μJy cps^{-1}. The unabsorbed flux after $t \approx 300$ s until $t \approx 550$ ks is $F_E = (2.6 \pm 0.4) \times 10^{-5} (t/[10^3 \mathrm{s}])^{-1.37 \pm 0.03}$ μJy. We find that the afterglow flux at $t = 10$ h is $F_{\mathrm{X,10}} \approx 6.0 \times 10^{-14}$ erg s^{-1}, which at a redshift of $z = 0.457$ gives a luminosity of $L_{\mathrm{X,10}} = 4.6 \times 10^{43}$ erg s^{-1}. Assuming that this flux comes from an adiabatically expanding external shock in the slow-cooling regime, the expected (unabsorbed) R-band optical flux is a factor ≈ 20–520 times higher, depending on the location of the cooling break below the X-ray band (e.g. Sari, Piran & Narayan 1998).

The resulting BAT and XRT detections are plotted in blue and red, respectively, in Fig. 1. The expected optical flux from the forward shock falls within the grey region shown in the plot. Our optical observations discussed below rule out a bright optical afterglow for this event, although a cooling break located just below the XRT bandpass would allow for optical emission to have gone undetected and still fit within the framework of the standard external shock afterglow model. The lack of a bright optical afterglow for GRB 070724A is consistent with the trend for low-fluence bursts to have faint afterglows noted by Gehrels et al. (2008) and Nysewander, Fruchter & Pe'er (2008). This makes GRB 070724A particularly interesting because it allows for the search of SN-related optical emission without the need to contend with external shock powered afterglow emission.

2.2 Optical/NIR

Our earliest observations of the location of GRB 070724A were taken with the United Kingdom Infrared Telescope (UKIRT) at Mauna Kea, beginning with a 20 s exposure in the K band at 13:11 UT on July 7, roughly 2.3 h after the trigger. Several epochs of observations followed in the J, H and K bands over the next 24 h, ending approximately 1.1 d after the burst.

Our imaging campaign in the optical passbands began with the use of StanCam at the Nordic Optical Telescope (NOT) on La Palma/Spain starting at 04:18 UT, roughly 17.5 h after trigger. These observations consisted of 3×300 s in B and I bands and 3×600 s in the R band. Comparison images of 6×600 s in R were taken at 03:35 UT on 2007 August 16, 22.7 d after trigger.

We obtained an additional 600 s I-band image with the European Southern Observatory-Very Large Telescope (VLT) equipped with the FORS2 instrument starting at 09:08 UT (22.1 h after trigger), followed by spectroscopic observations, which will be described below.

Our most extensive observations of the error circle of GRB 070724A were performed using the ANDICAM instrument operated by the SMARTS consortium on the 1.3-m telescope at Cerro Tololo Inter-American Observatory. Optical/infrared (IR) imaging in J and I bands began at 08:14 UT (21.3 h after trigger) and continued for an additional eight epochs with the last observations occurring at 07:31 UT on August 21 (27.8 d post trigger). Several dithered images were obtained in each filter, with total summed exposure times of 30 min in J and 36 min in I.

Finally, we obtained deep optical imaging with the 10-m Keck I Telescope equipped with the low-resolution imager and spectrograph (LRIS) instrument (Oke et al. 1995) at Mauna Kea, starting at 13:40 UT on August 11. The co-addition of successive observations yields a total effective exposure time of 2720 s in R and 2120 s in the g' band, followed by spectroscopic observations, which will be described below. All observations were conducted under photometric conditions and zero-pointing was performed using a standard star field observed at a similar airmass.

2.3 Photometry

All of our observations were reduced using standard CCD packages in IRAF. Once reduced, the co-addition of successive observations was performed using the SWARP and SHIFTADD software packages[3] to produce weighted sum images of the host field. Astrometry was performed relative to United States Naval Observatory-B1 using at least 15 sources in common between our summed image and the catalogue.

A custom pipeline was then used to perform photometry on individual and co-added frames, using aperture photometry via the SEXTRACTOR software package (Bertin & Arnouts 1996), to estimate instrumental magnitudes. An aperture size of $6/5 \times$ seeing [(full width at half-maximum (FWHM)] was used for the analysis across all our science data. Our instrumental magnitudes were then compared to a standard star field typically taken on the night of each observation for zero-point determination of each reduced frame. The aperture size used to photometrize the standard star frames was typically two to three times larger than the aperture used in the analysis of particularly deep, and hence crowded, images. For these images, an aperture correction was applied to account for the differing aperture radii.

To search for afterglow emission and to properly account for the host galaxy contribution, we employ a modified version of the public POIS-IPP package.[4]

Using the last image in each instrument series as a template of the host, we find no evidence for residual afterglow emission. Subtractions employed on images spanning much smaller timescales and taken with other facilities likewise show no signs of variability between observations. A subtraction between the co-addition of all R-band Keck observations taken 18 d after trigger and a 30-min exposure taken 1 yr after the event can be seen in Fig. 3.

We estimate the limiting magnitudes on these observations by placing 1000 blank apertures at random positions on the images. We take the standard deviation of the resulting photometry distribution to represent the counts associated with the sky noise of that image and assume that the faintest observable object is three times this value for a 3σ limiting magnitude. The limiting magnitudes as a function of position on the host galaxy were calculated by taking this theoretical limiting magnitude due to the sky and adding in quadrature the error associated with the counts from the galaxy at a given pixel, which were assumed to be Poissonian and therefore $\propto \sqrt{N}$. The resulting spatially resolved limiting magnitudes are shown as a contour plot in Fig. 2. We check these estimates by placing fake stars with a magnitude near our estimated limiting magnitudes in a subset of our frames and then test whether they would be detectable at varying thresholds above background.

---

[3] http://terapix.iap.fr/rubrique.php?id_rubrique=49
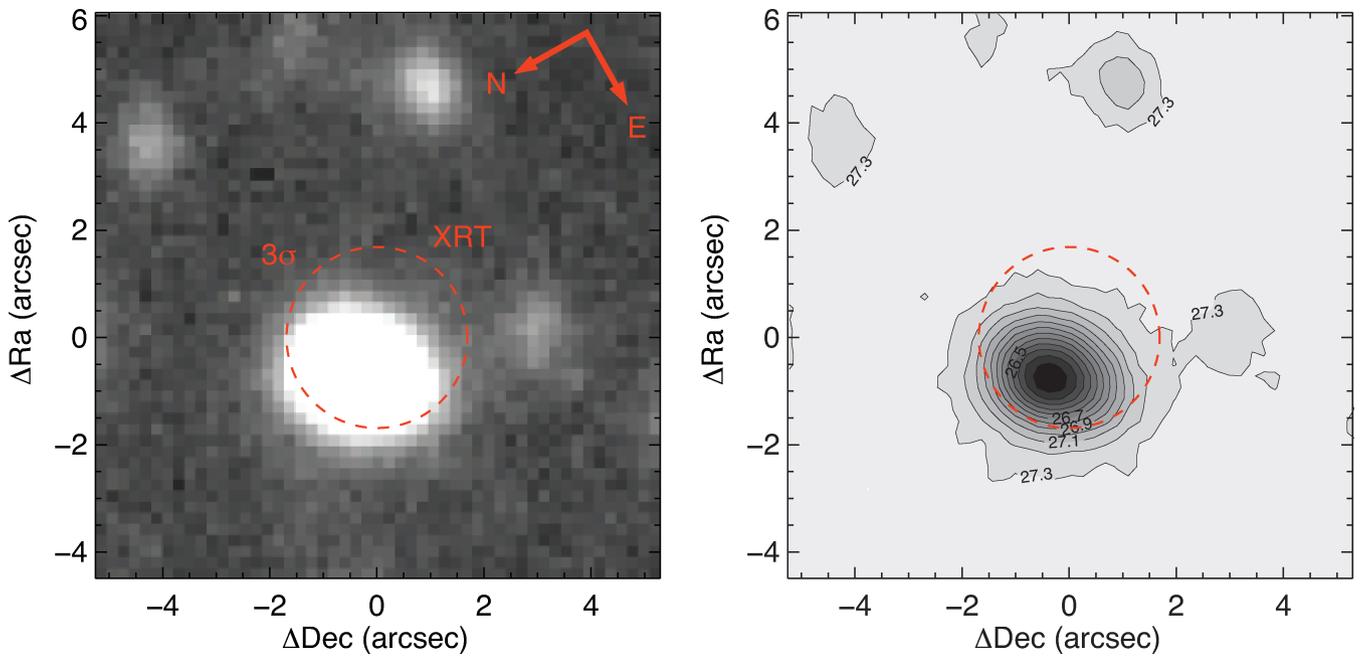[4] http://pan-starrs.ifa.hawaii.edu/project/IPP/software/

Figure 2. Left-hand panel: stacked Keck *R*-band image (taken 18 d after the event) of the region around the putative host galaxy. The 3σ XRT error circle is plotted in red. Right-hand panel: spatially resolved limiting magnitude contour map, derived after removing an elliptical isophotal model for the host.
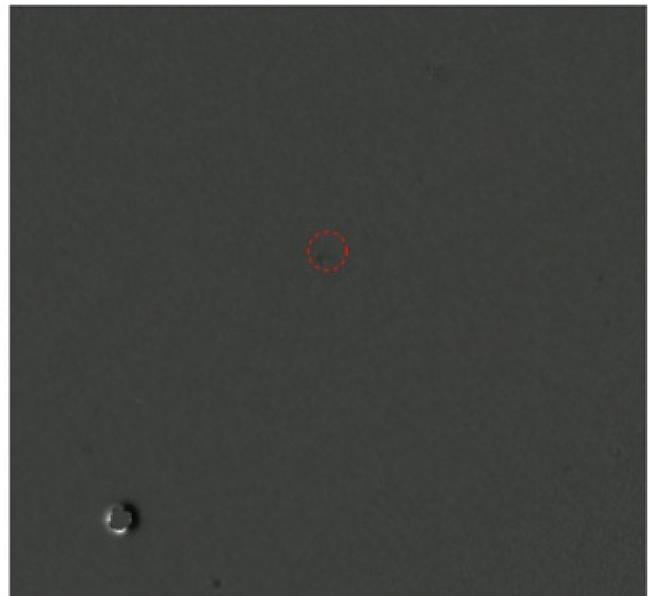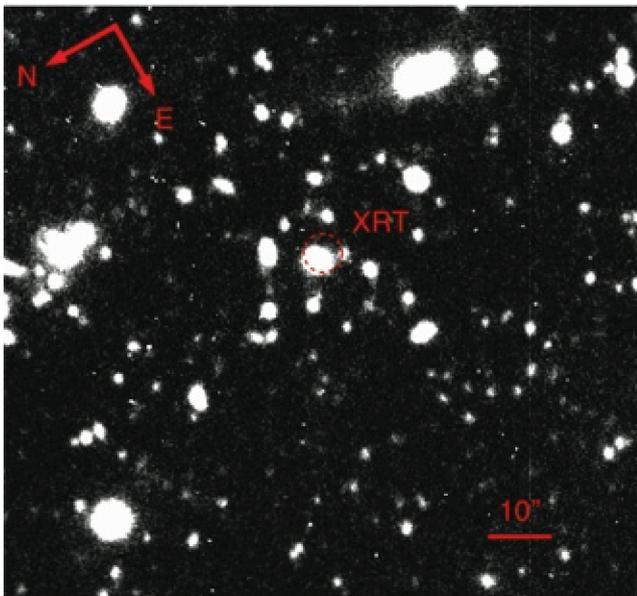

Figure 3. Left-hand panel: stacked Keck *R*-band image (taken 18 d after the event) of the region around the putative host galaxy. The 3σ XRT error circle is plotted in red. Right-hand panel: the subtraction of the same field observed 1 yr after the event showing no significant sources at the position of the XRT position. Similar subtractions were performed for all multi-epoch observations that spanned more than 1 d.

The summary of the optical/near-infrared (NIR) observations and their associated upper limits can be found in Table 1. Fig. 1 shows the upper limits at different epochs along with the BAT and XRT detections. Our early *R*-band observations taken with the NOT at ∼0.73 d effectively rule out any emission originating from the forward shock in the context of the canonical fireball model.

2.4 Spectroscopy

We obtained a single 900-s spectrum (henceforth called 'slit 1') of the host galaxy (Bloom 2007) of GRB 070724A with LRIS at the Keck I telescope, Mauna Kea, Hawaii, on 2007 August 11. The spectrum covers the wavelength range between 3500 and 9400 Å. A slitwidth of 1.0 arcsec and grism 600/4000 were used in the blue, providing a resolution of 4.0-Å FWHM. In the red, a grism 400/8500 was used providing a resolution of ∼6.5-Å FWHM. The spectra were extracted and wavelength calibrated using standard tools in IRAF. All wavelengths given are in air. Flux calibration was done using the spectrophotometric standard star BD+174708. The longslit covered both the host galaxy and a neighbouring galaxy to the south-west of the host galaxy at similar redshift (hereafter G3). Note that the narrow slit of 1.0 arcsec does not contain the entire

Table 1. Photometric observations of GRB 070724A.

Day	Instrument	Filter	Exp (s)	Limiting magnitude	Flux (μJy)
0.0961	UKIRT/UFTI	K	540	18.05	40.17
0.1057	UKIRT/UFTI	J	405	19.62	22.54
0.1270	UKIRT/UFTI	H	270	18.88	28.65
0.1316	UKIRT/UFTI	K	540	18.35	30.36
0.7254	NOT/StanCam	i	900	23.47	1.38
0.7384	NOT/StanCam	R	1800	23.72	1.01
0.7640	NOT/StanCam	B	900	21.95	6.82
0.8896	CT1.3m/ANDICAM	J	60	20.67	8.59
0.8897	CT1.3m/ANDICAM	I	360	21.79	4.69
0.9271	VLT/FORS	i	119	24.74	0.31
1.1270	UKIRT/UFTI	K	1440	17.47	68.53
2.8488	CT1.3m/ANDICAM	J	1800	20.80	7.59
2.8488	CT1.3m/ANDICAM	I	2160	21.95	4.04
4.9158	CT1.3m/ANDICAM	J	1800	19.16	34.27
4.9158	CT1.3m/ANDICAM	I	2160	21.85	4.43
6.9235	CT1.3m/ANDICAM	J	1800	19.46	26.13
6.9235	CT1.3m/ANDICAM	I	2160	21.90	4.24
9.9057	CT1.3m/ANDICAM	J	1800	19.93	16.94
9.9057	CT1.3m/ANDICAM	I	2160	20.70	12.71
13.9056	CT1.3m/ANDICAM	J	1800	19.99	15.96
13.9008	CT1.3m/ANDICAM	I	2160	21.71	5.03
16.9389	CT1.3m/ANDICAM	I	2160	21.83	4.50
18.1155	Keck I/LRIS	R	300	25.10	0.28
18.1155	Keck I/LRIS	g′	30	23.32	1.70
18.1221	Keck I/LRIS	R	10	23.39	1.37
18.1237	Keck I/LRIS	R	10	23.26	1.54
18.1257	Keck I/LRIS	R	600	25.39	0.22
18.1307	Keck I/LRIS	g′	200	25.00	0.36
18.1341	Keck I/LRIS	R	600	25.37	0.22
18.1342	Keck I/LRIS	g′	630	25.50	0.23
18.1422	Keck I/LRIS	g′	630	25.70	0.19
18.1423	Keck I/LRIS	R	600	25.44	0.21
18.1506	Keck I/LRIS	R	600	25.44	0.21
18.1506	Keck I/LRIS	g′	630	25.80	0.17
18.1416	Keck I/LRIS	R	2720	27.40	0.03[a]
18.1460	Keck I/LRIS	g′	2120	26.25	0.12[b]
20.9249	CT1.3m/ANDICAM	J	1800	19.77	19.76
20.9250	CT1.3m/ANDICAM	I	2160	21.33	7.13
22.6958	NOT/StanCam	R	3600	24.80	0.37
23.8962	CT1.3m/ANDICAM	J	1800	20.00	15.95
23.8962	CT1.3m/ANDICAM	I	2160	21.63	5.43
25.9324	CT1.3m/ANDICAM	J	1800	20.02	15.65
25.9324	CT1.3m/ANDICAM	I	2160	21.67	5.20
27.8593	CT1.3m/ANDICAM	J	1800	20.21	13.10
27.8593	CT1.3m/ANDICAM	I	2160	22.11	3.48

Note. We assume a T_0 of 10:53:50 on 2007 August 24.
[a]Co-addition of all R-band Keck observations.
[b]Co-addition of all g′-band Keck observations.

Figure 4. Field around the host galaxy of GRB 070724A and positions of the slits. The galaxies in the field with measured redshifts are indicated according to the notation in Table 3.

the north–south direction and therefore covered a slightly different part of the host galaxy. The other objects in the slit do not show any obvious emission lines. Reduction and calibrations were also performed with IRAF standard tasks and flux calibration performed using the spectrophotometric standard LTT9239. In contrast to the LRIS spectra, wavelengths for the FORS spectrum are in vacuum.

The position of the slits and the field around the host of GRB 070724A can be seen in Fig. 4.

3 THE HOST GALAXY AND ITS NEIGHBOURS

The XRT position of GRB 070724A, with an error radius of 1.6 arcsec, is offset by roughly 0.8 arcsec from the centre of a $z = 0.456$, 19.55 R-band magnitude, galaxy that we identify as the host galaxy. Following the formalism for small offsets (appendix B in Bloom et al. 2002), we estimate that the chance alignment of a burst given this redshift, offset and host magnitude is exceedingly small, roughly $P = 0.002$. At this redshift, the projected offset would transform to a physical distance of 5 kpc from the centre of the galaxy although this value is largely unconstrained due to the relative size of the projected offset to the XRT error radius. Offsets of the order of a few kpc have been seen previously in some short bursts, though much larger offsets have frequently been reported (Bloom et al. 2007; Troja et al. 2008). As short GRBs are assumed to originate from the merger of two compact objects, the kick from the SNe explosions could lead to large offsets from their birthplace and their host galaxies, which seems to agree with the observations (e.g. Bloom, Sigurdsson & Pols 1999; Fryer, Woosley & Hartmann 1999; Belczynski et al. 2006). No other bright sources have been found within or near the XRT position; however, two galaxies at a similar redshift have been discovered at a distance of several arcsec from the GRB position. We analyse the properties of these galaxies together with the host galaxy in this section (see also Section 3.2).

Fig. 5 shows the spectra of the host as well as all galaxies where the redshift could be determined, named G2, G3, G4 and G5 in Fig. 4.

flux for both galaxies, which affects later analyses derived from the flux calibrated spectra.

Furthermore, we obtained spectra with LRIS at three other slit positions on 2007 October 10 and 11, with the same setting and calibrated with the standard star Feige 110. The three slits (slits 3, 4 and 5) cover a number of galaxies of which only three show strong emission or absorption lines allowing for redshift determinations.

We also obtained a 600 s spectra with FORS1 (called 'slit 2') at the VLT on Cerro Paranal, Chile, on 2007 July 25, starting 09:52 UT using grism 300V and a 1.0 arcsec slit, which has a resolution of 11 Å FWHM. Due to heavy fringing, the emission lines of the host are not detected with high significance. The slit was positioned in
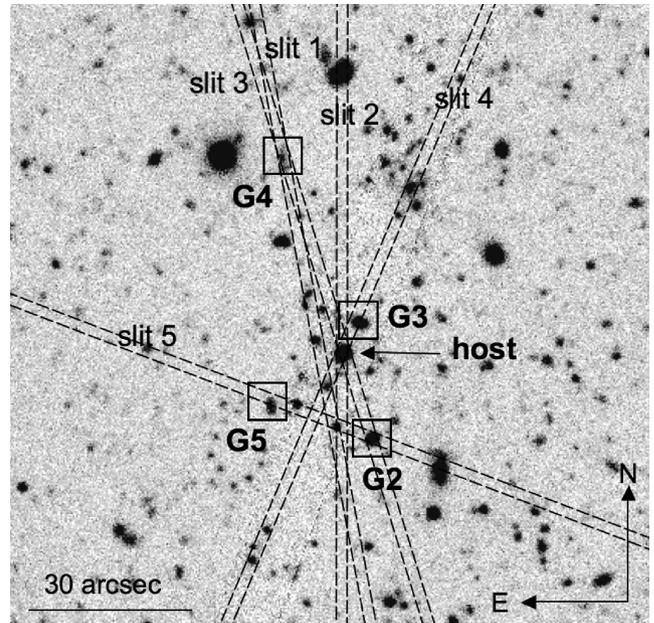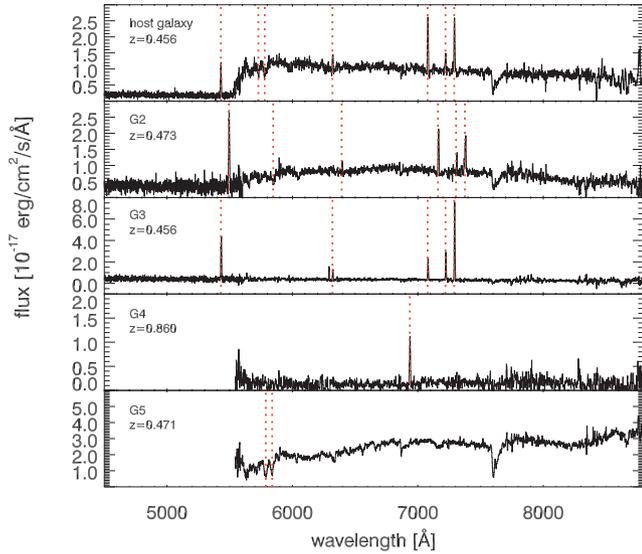
Figure 5. Spectra of the host galaxy and some of its neighbours with determined redshifts. The lines indicated correspond to the lines noted in Table 3.

3.1 Properties of the host

The star-forming nature of the host galaxy is suggested by the detection of several emission lines in the spectra, including [O II] $\lambda\lambda$ 3727, 3829, [O III] $\lambda\lambda$ 4959, 5007, Hβ and Hγ as well as the Ca H and K absorption lines. Unfortunately, the redshift of $z = 0.456$ places Hα at ~9600 Å outside the wavelength range of our spectra. In Table 2, we give the emission-line values for the two different slit positions, which probe slightly different regions, where 'slit 1' indicates the Keck observation and 'slit 2' indicates the position of the FORS observation (in the north–south direction). All other slits shown in Fig. 4 were observed with Keck.

Using the detected emission lines in slit 1 and slit 2, we can derive a number of properties, including the extinction, star formation rate (SFR) and metallicity of the star-forming regions. As Hα is not available for extinction measurements using the Balmer-line decrement (Osterbrock 1989), we use the ratio between Hγ and Hβ, which is 0.47 (for $T_e = 10^4$ K, $n_e = 100$ cm^{-3}) in the absence of any extinction. Unfortunately, Hγ is not observed in slit 2, likely due to the lower signal-to-noise ratio, so we rely solely on the slit 1 for our extinction estimates. Using the measured line fluxes for slit 1 shown in Table 2 and assuming $R_V = 3.1$ and the Cardelli, Clayton & Mathis (1989) extinction curve, we obtain a reddening value of $E(B - V) = 1.2 \pm 0.2$ mag. The Galactic reddening along the line of sight towards the host is only $E(B - V) = 0.013$ mag

Table 2. Photometric observations of the host galaxy of GRB 070724A.

Instrument	Filter	Magnitude	Flux (µJy)
NOT/StanCam	B	21.12	9.12
Keck I/LRIS	g'	21.64	8.02
Keck I/LRIS	R	19.56	46.56
CT1.3m/ANDICAM	I	20.01	24.32
UKIRT/UFTI	J	18.90	43.25
UKIRT/UFTI	H	18.70	34.67
UKIRT/UFTI	K	17.70	54.45

(Schlegel, Finkbeiner & Davis 1998). From the detection of the Ca break and the shape of the spectrum, we conclude that the galaxy has an underlying stellar older population which contributes some absorption in the Balmer lines. This affects Hγ more than Hβ, which, if we were able to correct for it, would lead to a lower value for the extinction. Due to the low resolution of the spectrum, we are not able to determine the strength of the stellar absorption.

The SFR can be obtained from the Hα or the [O II] $\lambda\lambda$ 3727, 3729 line flux using the conversion from Kennicutt (1998). Hα is outside of our spectral range, and we therefore use [O II], which has a more indirect connection to the ongoing SFR than Hα. Taking the unextincted values, we then obtain an absolute SFR of 0.83 ± 0.03 M$_\odot$ yr^{-1} from the Keck slit (slit 1) and a specific SFR scaled with the g-band magnitude of 21.75 mag (at $z = 0.456$ equal to the rest-frame u band) of 1.64 M$_\odot$ yr^{-1} $(L/L^*)^{-1}$ assuming that an L^* galaxy has an absolute magnitude of $M_B = -21$ mag (Christensen, Hjorth & Gorosabel 2004). The extinction-corrected fluxes give a rather high absolute SFR or 129 ± 4 M$_\odot$ yr^{-1} (the errors from the extinction correction are not propagated) and an SSFR of 253 M$_\odot$ yr^{-1} $(L/L^*)^{-1}$. Due to the stellar absorption in the Balmer lines mentioned above, the true SFR lies in between the unextincted and the extinction-corrected values.

Using the R_{23} parameter, which takes the ratio of the [O II], [O III] and Hβ emission-line fluxes (uncorrected for possible extinction in the host), we derive a metallicity for the host galaxy. The most frequently applied calibration for GRB hosts is the one taken from Kewley & Dopita (2002), which gives a rather high metallicity of $12 + \log(O/H)_{KD02} = 9.1$ for this galaxy as compared to the solar metallicity value of 8.66 (Asplund et al. 2004). Using the extinction-corrected fluxes leads to the same value for the metallicity. The intrinsic error of this method for determining the metallicity is around 0.2 dex.

The Hβ equivalent width (EW) is dependent on the age of the stellar population and can be used as an upper limit for the age according to stellar evolutionary models (e.g. Leitherer et al. 1999). A value of $\log(EW_{H\beta}) = 1.04$ or 1.22 for the two slit positions corresponds to an age of about 10 Myr for an instantaneous starburst and about 100 Myr for continuous star formation depending slightly on the metallicity. The Balmer break, which is clearly visible in the spectrum of the host galaxy, furthermore indicates an age of at least 100 Myr, indicating an older population of stars. This is consistent with the photometry for this host and quite interesting given the detection of strong emission features. It could indicate recent starburst activity, possibly due in part to a merger event with one of its nearby neighbours, revitalizing what was otherwise an old, red galaxy.

3.2 Is the host part of a cluster?

Since the first well-localized SHB (GRB 050509b) was found to be in a cluster (Bloom et al. 2006), the frequency of SHBs in clusters has been a subject of study (Berger et al. 2006). To investigate the potential for diffuse X-ray emission from a cluster of galaxies, we search for extended sources using WAVDETECT (Freeman et al. 2002). We analysed the X-ray data on scales of 0.8, 1.1, 1.6, 2.2, 3.1 arcmin and found no strong detections which are not centred on point sources in the 91.7 ks exposure XRT PC mode image (detections centred on point sources are considered suspect due to the broad wings of the XRT point spread function). Assuming a thermal bremsstrahlung spectrum with $kT = 5.0$ keV (e.g. Bloom et al. 2006) at $z = 0.457$, any cluster must be fainter than 2×10^{43} erg s^{-1}

Table 3. Emission-line measurements for the host and the neighbouring galaxy.

Line	λ_{obs} (Å)	z	EW (Å)	Flux (measured) (10^{-17} erg cm^{-2} s^{-1})	Flux (corrected) (10^{-17} erg cm^{-2} s^{-1})
Host galaxy					
[O II] $\lambda\lambda$ 3727,29	5429.85	0.4562	–	7.75 ± 0.22	1198 ± 34
Ca H λ 3934	5729.02	0.4564	3.89 ± 0.48	–	–
Ca K λ 3969	5782.62	0.4571	8.98 ± 0.58	–	–
Hγ 4340	6321.95	0.4565	–	4.22 ± 0.39	388 ± 36
Hβ 4861	7079.83	0.4564	16.94 ± 0.78	15.40 ± 0.10	851 ± 6
[O III] 4959	7221.33	0.4562	–	4.86 ± 0.62	244 ± 31
[O III] 5007	7291.92	0.4564	–	14.1 ± 0.6	674 ± 29
Host, slit 2					
[O II] $\lambda\lambda$ 3727,29	5433.84	0.4568	–	24.9 ± 0.15	–
Ca H λ 3934	5732.19	0.4568	3.03 ± 0.19	–	–
Ca K λ 3969	5787.39	0.4579	8.82 ± 0.21	–	–
Hβ 4861	7084.36	0.4569	11.09 ± 0.95	7.29 ± 0.62	–
[O III] 4959	7225.96	0.4567	–	4.03 ± 0.41	–
[O III] 5007	7293.97	0.4564	–	10.2 ± 1.2	–
G2					
[O II] $\lambda\lambda$ 3727,29	5493.76	0.4733	–	8.57 ± 0.53	526 ± 33
Ca K λ 3969	5849.10	0.4738	8.89 ± 2.32	–	
Hγ 4340	6396.06	0.4735	–	2.73 ± 0.24	110 ± 9
Hβ 4861	7163.21	0.4735	15.92 ± 0.66	8.93 ± 0.37	236 ± 10
[O III] 4959	7307.87	0.4736	–	2.98 ± 0.36	73 ± 9
[O III] 5007	7378.33	0.4736	–	10.4 ± 0.36	244 ± 9
G3					
[O II] $\lambda\lambda$ 3727,29	5432.39	–	0.4568	31.3 ± 1.5	–
Hγ 4340	6322.35	0.4566	–	6.69 ± 0.31	–
Hβ 4861	7081.26	0.4567	46.12 ± 1.02	13.6 ± 0.3	–
[O III] 4959	7223.49	0.4567	–	17.7 ± 0.5	–
[O III] 5007	7293.41	0.4567	–	54.8 ± 0.5	–
G4					
[O II] $\lambda\lambda$ 3727,29	6937.05	0.8604	–	9.25 ± 0.07	–
G5					
Ca H λ 3934	5787.39	0.4712	18.54 ± 1.21	–	–
Ca K λ 3969	5837.22	0.4709	15.49 ± 1.08	–	–

(3σ). This is an order of magnitude fainter than the rich X-ray cluster associated with GRB 050509B.

We determined the redshift of the galaxies around the host in order to determine a possible group or cluster as found for two other SHBs (Berger et al. 2007). For most of the galaxies in the slit, we could not determine any redshift due to a lack of strong emission or absorption lines. We did not attempt to determine redshifts via spectral energy distribution (SED) modelling of the spectral shape for these sources, as such a method would not have yielded the necessary redshift accuracy to determine whether the galaxies could belong to a cluster or a group connected to the host galaxy.

We find that the galaxy about 5 arcsec north-west of the host, called G3 in Fig. 4 and Table 3, has the same redshift as the host. Also the galaxies G2 and G5, which are about 10–20 arcsec from the host both have a similar redshift of $z = 0.473$ and 0.471. However, this would correspond to a distance of 57–115 kpc from the host to G2+G5, which makes it unlikely that the host+G3 are gravitationally bound to G2+G5. G4 only shows one emission line which, if associated with O II, would give a redshift of $z = 0.860$. Together with the X-ray observations, we therefore conclude that the host may be a member of a smaller group but does not belong to a larger cluster.

3.3 Properties of surrounding galaxies

A small number of the galaxies probed by the different slits show prominent emission or absorption lines for the remaining galaxies. The only galaxy which was identified to have the same redshift as the host galaxy, G3, has a young stellar population. Its spectral slope is rather flat and does not show any 4000 Å Balmer break. There is also no detection of the Ca II absorption lines. The Hβ EW suggests an age between 4 and 20 Myr, and only one of the Ca II lines could be clearly identified. G2, which has a slightly higher redshift than the host, shares some of its properties, with a moderate Hβ EW indicating an age between 10 and 100 Myr and a clear 4000-Å break. However, only one of the Ca II absorption lines could be clearly identified. G4 has only one emission line likely identified with the O II doublet, which indicates a younger stellar population. G5 has no emission lines but clear Ca II absorption and a Balmer break, which suggests an older galaxy.

We utilize the same methods to determine the SFR, extinction and metallicity as those described in the previous section to determine the properties of the other galaxies probed by the different slits. For G2, we get an extinction from the Balmer-line ratio between Hβ and Hγ of $E(B − V)_{G2} = 0.96 \pm 0.7$ mag. From the flux of

[O II] λ 3729, we obtain an SFR_{G2} of $1.0 \pm 0.1 \, M_\odot \, yr^{-1}$ or an SSFR of $3.38 \, M_\odot \, yr^{-1} \, (L/L^*)^{-1}$, the extinction-corrected fluxes give an SFR_{G2} of $61.4 \pm 3.8 \, M_\odot \, yr^{-1}$ or an SSFR of $207 \, M_\odot \, yr^{-1} (L/L^*)^{-1}$. The metallicity, assuming the upper branch solution, expected for an older galaxy, is high and very similar to that of the host galaxy with $12 + \log(O/H)_{G2} = 9.05$ (Kewley & Dopita 2002) or 8.9 using the extinction-corrected fluxes. For G3, we find that the extinction is consistent with zero, which agrees with the indications of a young, star-forming galaxy, although dusty starburst galaxies have been observed as well. The G3 SFR from [O II] is $3.4 \pm 0.1 \, M_\odot \, yr^{-1}$ with an SSFR of approximately $21.2 \, M_\odot \, yr^{-1}$ $(L/L^*)^{-1}$ and the metallicity of either $12 + \log(O/H)_{G3} = 8.23$ for the lower branch solution or $12 + \log(O/H)_{G3} = 8.61$ for the upper branch, which in both cases would imply subsolar metallicities. For a clear determination of the metallicity, the detection of Hα or the temperature sensitive line [O III] λ 4363 would be necessary (Izotov et al. 2006). In case the emission line identified in G4 is [O II] λ 3727, 3729, we get an SFR_{G4} of $4.7 \pm 0.1 \, M_\odot \, yr^{-1}$ or an SSFR of $47.0 \, M_\odot \, yr^{-1} \, (L/L^*)^{-1}$.

4 CONSTRAINTS ON EXCESS OPTICAL EMISSION

4.1 Constraints on an associated core-collapse supernova

Through the use of our non-detection of the optical afterglow, we can derive limits on the optical contribution from SN of Type Ib or Ic associated with this event. In Fig. 6, we plot three different SN Ic templates together with the upper limits in the R band. In order to convert our photometry to rest-frame values (k-correction), we fit the SED (in flux units) derived from data points and interpolations of the $UBVRI$ light curve for each day, redshifting the SED to $z = 0.456$, and determined the new fluxes at the effective R-band wavelength before transforming these flux values back into magnitudes. Furthermore, the templates were corrected for time dilation as well as for Galactic extinction. The comparison templates used are the 'standard' long-duration GRB–SN 1998bw (Galama et al. 1998), an SN associated with an X-ray flash (XRF), SN 2006aj (Sollerman et al. 2006) and faint Type Ic SNe 2002ap (Foley et al. 2003) and 1994i (Richmond et al. 1996). All observed SNe that have been as-
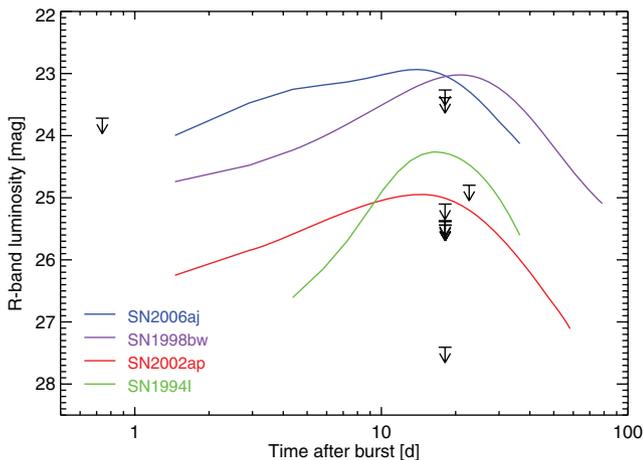

Figure 6. Different SN Ic and GRB–SN templates as they would appear shifted to $z = 0.456$, the redshift of the host galaxy. The SN light curves are time dilated accordingly, the magnitudes are corrected for the luminosity distance after applying a k-correction by fitting the SEDs at different times. The templates are not corrected for possible extinction in the SN host galaxy.

sociated with a long-duration GRB are within 0.5 mag of the peak luminosity of SN 1998bw, although some XRF-SNe have appeared to be significantly fainter, possibly because of dust (Soderberg et al. 2006; see also Woosley & Bloom 2006).

Taking the deep limit in the R band from Keck I on 2007 August 11, of $R = 27.4 \, mag \, (2\sigma)$, any broad-line SN Ic associated with this short GRB would have been at least 100 times fainter than SN 1998bw and still 10 times fainter than SN Ic 1997ef. If the extinction in the host galaxy is indeed as high as derived in Section 3.1, a very faint SN Ic could indeed have been missed, SN 1998bw would, however, still have been brighter than the observed limits.

4.2 Li–Paczyński modelling

Our observations also allow us to place limits on the optical emission from a so-called 'mini-SN' or LP-SN (Li & Paczyński 1998; Rosswog & Ramirez-Ruiz 2002; Kulkarni 2005). In this model, the coalescence of two compact objects produces a sub-relativistic ejecta of nuclear dense material comprising approximately 10^{-4}–$10^{-2} \, M_\odot$, depending on the nuclear equation of state and the properties of the merger (such as nature of the components and initial mass ratio). The rapid decompression of the ejecta as it expands adiabatically is thought to result in the synthesis of a variety of radioactive elements, which could decay over a wide range of time-scales. With nominal and simplistic assumptions, the spectrum of such emission is expected to be quasi-thermal and peak in the optical/UV range with a characteristic time-scale of about 1 d.

Using the simple derivations presented in Li & Paczyński (1998), we can construct an analytic model to describe the properties of this LP-SN light curve as a function of three parameters: the mass, M, and velocity, βc, of the ejecta, and the fraction of the ejecta energy, f, that goes into radioactive decay per e-fold in time over the relevant time-scales. Following Li & Paczyński (1998), the peak luminosity, time to reach this value and effective temperature of the ejecta can be given, respectively, as

$$L_{pk} = 2.1 \times 10^{44} \, erg \, s^{-1}$$
$$\times \left(\frac{f}{0.001} \right) \left(\frac{M}{0.01 \, M_\odot} \right)^{1/2} (3\beta)^{1/2} \left(\frac{\kappa}{\kappa_e} \right)^{-1/2}, \quad (1)$$

$$t_{pk} = 0.98d \left(\frac{M}{0.01 \, M_\odot} \right)^{1/2} (3\beta)^{-1/2} \left(\frac{\kappa}{\kappa_e} \right)^{1/2} \quad (2)$$

and

$$T_{eff,pk} = 2.5 \times 10^4 \, K$$
$$\times \left(\frac{f}{0.001} \right)^{1/4} \left(\frac{M}{0.01 \, M_\odot} \right)^{-1/8} (3\beta)^{-1/8} \left(\frac{\kappa}{\kappa_e} \right)^{-3/8}. \quad (3)$$

Here κ is the average opacity (κ_e is the opacity caused by electron scattering). The time of peak luminosity occurs when the photons can diffuse outwards on the dynamical time, so that most of the thermal energy that is produced by the radioactive decay can be radiated efficiently before suffering significant adiabatic cooling. Since the photon diffusion time is $\sim\tau$ times larger than the source light crossing time, R/c, and $R = \beta ct$, we can equate the dynamical time $t_{dyn} \sim t = R/\beta c$ with $\tau R/c$ at t_{pk} and therefore $\beta^{-1} \sim \tau(t_{pk}) \propto \kappa M/(\beta t_{pk})^2$ and $t_{pk} \propto (\kappa M/\beta)^{1/2}$. The peak luminosity is approximately given by $L_{pk} \sim f M c^2/t_{pk} \propto f(\beta M/\kappa)^{1/2}$, and the effective temperature is obtained by equating this luminosity to that of a blackbody, $L_{pk} \sim 4\pi R^2(t_{pk})\sigma T_{eff,pk}^4 = 4\pi(\beta ct_{pk})^2\sigma T_{eff,pk}^4$ and therefore $T_{eff,pk} \propto L_{pk}^{1/2}(\beta t_{pk})^{-1/2} \propto f^{1/4}\kappa^{-3/8}(\beta M)^{-1/8}$.

As a result, the luminosity of the resulting light curve is directly proportional to the fraction of the ejecta energy that goes into radioactive decay (i.e. the ejecta efficiency). An increase in the assumed mass in the ejecta has the effect of both increasing the total luminosity of the emission as well as increasing the time, t_{pk}, to peak luminosity, L_{pk}. On the other hand, an increase of ejecta velocity leads to an increase in the peak luminosity but a decrease in the peak duration.

The most efficient conversion of nuclear energy to observable luminosity is provided by elements with a decay time-scale comparable to the time-scale it takes the ejected debris to become optically thin, t_τ. In reality, there is likely to be a large number of nuclides with a very broad range of decay time-scales. The ejecta is optically thick at early stages, but its optical depth falls rapidly as the ejecta expands. As this happens, radiative losses at the photosphere become important, and the peak emission occurs when the optical depth reaches $\sim 1/\beta$. Current observational limits thus place interesting constraints on the abundances and the lifetimes of the radioactive nuclides that form in the rapid decompression of nuclear density matter – they should be either very short or very long when compared to t_τ so that radioactivity is inefficient in generating a high luminosity.

Fig. 7 shows the calculated R-band light curves for a range of ejecta mass M, velocity β and the fraction of the ejecta energy f that goes into radioactive decay, effectively the energy conversion factor. Plotted as black filled arrows are three R-band upper limits taken at roughly 0.74, 18.14 and 22.70 d from left to right. For comparison, we have also plotted the R-band upper limits for GRB 050509b presented by Hjorth et al. (2005a) and Bloom et al. (2006). Unfortunately, many of our observations between days 2 and 18 are less constraining, so that we can only place limits on a very fast, massive and highly efficient ejecta. Likewise, the deep upper limit at late time can only constrain a very slow, high-mass ejecta.

Also plotted as black hollow arrows are our *equivalent* limits if the optical emission from the LP-SN transient suffered the maximum ~ 3 mag of rest-frame R-band extinction that is implied by our measured reddening value of $E(B - V) = 1.2 \pm 0.5$ mag. The LP-SN could have been significantly brighter and have been missed
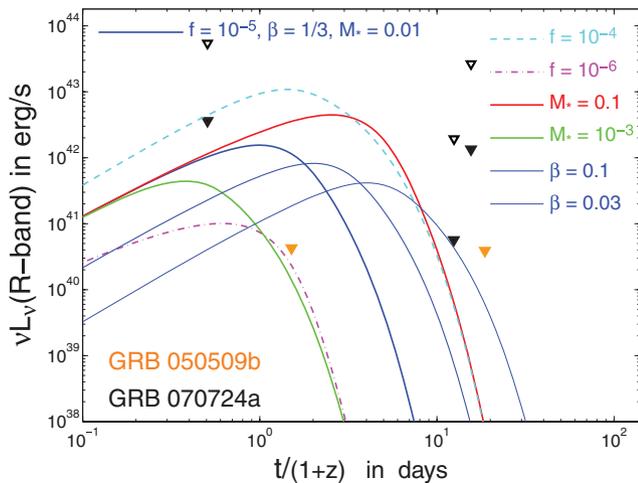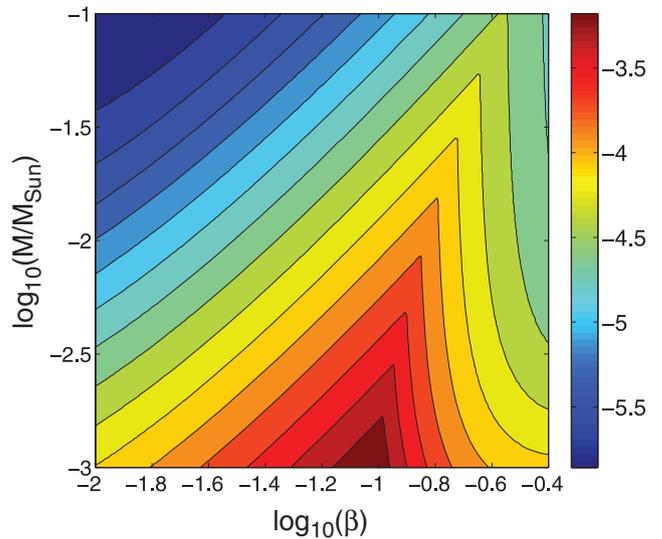

Figure 8. A parameter space plot for GRB 070724A showing the maximal allowed value that our observations place on the energy conversion factor f for a range of ejecta masses M and velocities β. For a given M_{ejecta} and β, the colour (coded at right) corresponds to the maximum allowed value for f.
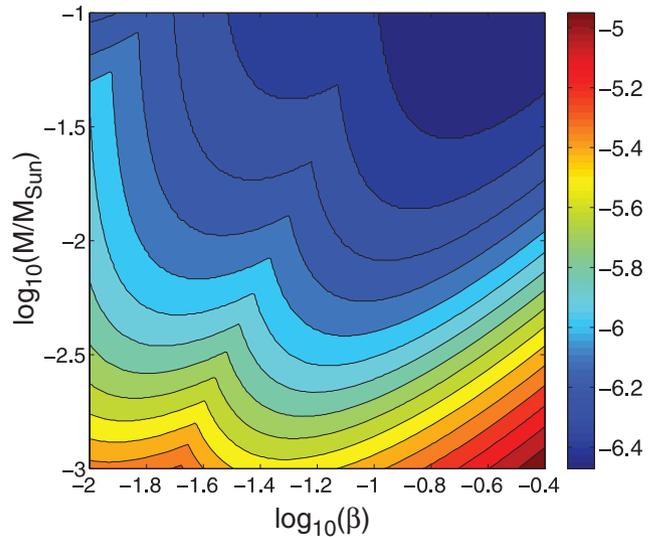

Figure 9. A parameter space plot for GRB 050509b showing the maximal allowed value that the observations made by Hjorth et al. (2005a) place on the energy conversion factor f for a range of ejecta masses M_{ejecta} and velocities β. For a given M_{ejecta} and β, the colour (coded at right) corresponds to the maximum allowed value for f.

by our search in this worst case scenario, allowing us to constrain only an extremely massive and highly efficient ejecta.

In Figs 8 and 9, we show the parameter space excluded by our observations for GRB 070724A as well as the upper limits on emission from GRB 050509b placed by Hjorth et al. (2005a). The areas in parameter space which are shown are divided into regions that are dominated by the constraint from a small number of upper limits. The dividing lines between these regions are demarcated by sharp changes in the direction of the contour lines.

In Fig. 8, the right to lower right side of the plot is dominated by the upper limit of 23.72 mag in the R band at 0.5068 d, while the other half of the plot is dominated by the upper limit of 27.4 mag

Figure 7. Li and Paczynski models for different ejecta masses M_*, velocities β and energy conversion factor f. Our R-band upper limits are shown in black filled arrows along with the upper limits presented by Hjorth et al. (2005a) for GRB 050509b. The black hollow arrows represent our equivalent limits if the optical emission from the LP-SN transient suffered ~ 3 mag of rest-frame R-band extinction.

in the *R* band at 12.44 d, both epochs listed in the host frame. The darker blue regions of the plot represent deeper limits on the fraction of the ejecta energy *f* that goes into radioactive decay. The parameter space that is least constrained represents the intermediate velocity ejecta at a wide range of masses. This corresponds to the time range for peak between days 2 and 18 for which we have only shallow upper limits in magnitude.

For comparison, the upper limits made by Hjorth et al. (2005a) place stricter limits on the presence of an LP-SN for GRB 050509b. The derived limits for GRB 050509b shown in Fig. 9 are dominated by the upper limit of 26.6 mag in the *R* band at 1.85 d (lower right) and by the upper limit of 27.5 mag in the *V* band at 3.92 d (upper left). At the very upper left corner (high *M* and low *β*), there is a small region which is dominated by the upper limit of 26.7 mag in the *R* band at 22.83 d. This is natural since $t_{pk} \propto (M/\beta)^{1/2}$ (see equation 2).

Finally, there is some ambiguity as to the time of origin in the LP-SN model, as the onset of the GRB and the onset of the LP-SN transient may not necessarily coincide. Although there is currently no theoretical prediction for this time lag, we can constrain delays of up to 10 d even for the moderately massive efficient ejecta under consideration in Fig. 7. Any such delay would have resulted in the detection of a bright transient during our deepest observation at 18.14 d post trigger. For an extremely inefficient ejecta (dash–dotted line), we can only constrain the delay in the onset of emission from 7–10 d post trigger. Alternatively, the late-time *R*-band limit on the LP-SN emission from GRB 050509b placed by Hjorth et al. (2005a) rules out a delay up to 11 d for all models under consideration in Fig. 7.

5 DISCUSSION

We present the results of a deep and extensive observing campaign of the short-duration hard spectrum GRB 070724A. Although our observations do not reveal an optical or NIR transient associated with this event, the derived upper limits can constrain optical emission from a traditional forward shock as well as the physical parameters of SNe or SNe-like models. Our early NOT and late-time Keck observations show no sign of the optical emission from a forward shock in the slow-cooling regime, as predicted by the fireball model. However, this optical contribution could have easily eluded detection given the weakness of the event combined with the potential extinction by the host galaxy.

Given the measured reddening value due to the host of $E(B - V) = 1.2 \pm 0.5$ mag, any optical emission could have suffered as much as $A_V \sim 4$ mag of extinction if the burst occurred well within the galaxy's core. In this case, the optical limits on a mini-SN quickly become unconstrained and our late-time observations would likewise barely constrain even most broad-lined Type Ic SNe. If the GRB exploded at a large offset to the host galaxy, as has been seen in other short-GRB events, or if the event occurred on the near side rather than the far side of the host, then much of the measured extinction would be largely irrelevant. The measured N_H could potentially help to resolve these different scenarios. Of the two *Swift* events which have solidly been shown to have $A_V > 3$, both have had large N_H column density at late times, of the order of 5×10^{22} cm^{-2} (Perley et al. 2009). We measure a similar column density at $t < 300$ s in association with large hardness variations in the X-ray detections, suggesting that the excess column density does not reflect the intrinsic absorption of the host. At late times ($t > 300$ s), the N_H value becomes consistent with the Galactic value $N_{H,Galactic} = 1.2 \times 10^{20}$ cm^{-2} (Dickey & Lockman 1990).

Furthermore, the extinction value is derived from emission-line measurement, indicating the extinction towards the regions of the galaxy that harbour younger populations of stars. These regions may differ greatly in their dust content from the extended disc or halo in which one would expect to find the older population of stars which are thought to be the progenitors of SHBs. Therefore, we conclude that the site of GRB 070724a was likely not affected by large amounts of extinction, although this remains a caveat in the proceeding discussion.

Because our limiting magnitudes are deepest at early and late times, our observations primarily constrain an efficient, very slow or a very fast ejecta with mass higher than 0.01 M$_\odot$. Our observations do little to exclude a low-mass ejecta at intermediate velocities resulting in emission reaching peak luminosity near 1 d. This can be seen in the case of GRB 050509b, where two limiting magnitudes in the *R* band are of similar depth although the earlier observation is far more constraining. This is due to the characteristic time-scales associated with the peak emission predicted by the LP-SN model. This underscores the importance of deep optical observations hours to days after the short-hard GRB. To be sure, our calculations are based on a very simplified analytic model, so it is not clear whether this basic result would hold for more realistic models (e.g. Kulkarni 2005).

We note that GRB 050509b and GRB 070724A represent the fainter end of the energetics distribution (Kann et al. 2008), at 2.40×10^{48} and 1.54×10^{49} erg, respectively, for short bursts thus far detected by *Swift*. If there is a correlation between the energy released in the prompt gamma-ray emission and the velocity and/or mass of the resulting ejecta, not an unreasonable scenario, then one would expect more energetic bursts to result in brighter emission from a mini-SN. Therefore, deep optical observations of more energetic SHB events may yet yield detectable emission.

To date, only 14 short bursts (GRB 050709, GRB 050724, GRB 051221A, GRB 060121, GRB 060313, GRB 061006, GRB 061201, GRB 070707, GRB 070714B, GRB 070809, GRB 071227, GRB 080503, GRB 080905A and GRB 090510) have resulted in the detection of an optical afterglow and therefore a position determined at subarcsecond level. Only four short GRBs detected thus far were proposed to be associated with early-type galaxies such as elliptical or early-type spiral galaxies, namely GRB 050509B (Gehrels et al. 2005; Bloom et al. 2006), GRB 050724 (Barthelmy et al. 2005; Berger et al. 2005; Gorosabel et al. 2006; Malesani et al. 2007) and possibly GRB 050813 (Berger 2006; Prochaska et al. 2006; Ferrero et al. 2007) and GRB 060502B (Bloom et al. 2006). The lack of emission lines in these galaxies implies low limits on any ongoing star formation, the age of their stellar populations is of the order of Gyr, and their metallicity is around solar. All other short-GRB hosts are late-type or irregular, star-forming galaxies, although with lower SFRs as compared to their long GRB host counterparts. The best studied examples of late-type galaxies associated with short bursts to date are the irregular host of GRB 050709 (Fox et al. 2005; Hjorth et al. 2005a; Covino et al. 2006) and the host of GRB 051221A (Soderberg et al. 2006).

The host galaxy of GRB 070724a is one of the growing number of star-forming galaxies to harbour a short GRB. Despite the lack of an optical detection, the position of the XRT error circle covering most of the galaxy makes an association very likely. The host galaxies of short bursts have been found to be a rather diverse population, in contrast to the more uniform sample of star-forming galaxies or at least star-forming regions within larger galaxies for long-duration GRB hosts (Christensen et al. 2004; Fruchter et al. 2006). Recently, Berger (2009) published properties for the full set of short-GRB
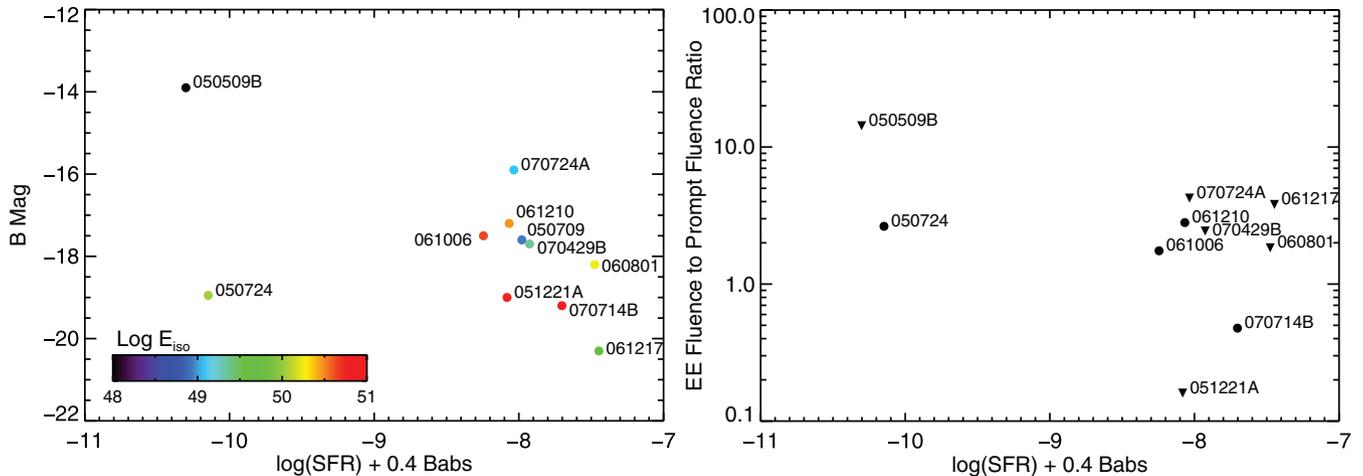
Figure 10. Left-hand panel: the R_c magnitude of the afterglow (or upper limit thereto) at 1 d after the GRB in a common $z = 1$ frame adopted from Kann et al. (2008) versus the specific SFR of the host galaxy as presented by Rhoads (2008). GRB 070724A represents the deepest limit on the existence of short time-scale SN-like emission for a short GRB in a moderately star-forming galaxy. The colour scheme represents the isotropic equivalent energy of the event. Right-hand panel: the ratio of the extended emission fluence to that of the initial spike (or the limit thereof) versus the host's specific SFR of a subset of short GRBs with known redshift. There is no clear connection between the events with significant extended emission and the properties of the host galaxy.

host galaxies, whose properties could be determined. They find that the range of SFRs is moderate with 1–$10 \, M_\odot \, yr^{-1}$, with some outliers with very low SFR, which is slightly lower than found for long-duration GRBs (e.g. Christensen et al. 2004). The metallicity is in general 0.6 dex (Modjaz et al. 2008) higher than for long-duration GRB hosts, however, this is based on a rather small sample for nearby long-duration GRBs. The host of 070724A has quite average properties compared to the short-GRB sample presented in Berger (2009) in terms of SFR and metallicity.

This diversity in both the host galaxy population and also the prompt energetics of short GRBs hints at the possibility of progenitors that may not be entirely restricted to the most widely favoured scenario involving the merger of compact binaries. The dichotomy between the specific SFRs of short-GRB hosts, in particular, has been proposed by Rhoads (2008) as a possible indication of multiple progenitors. Unlike the optical limits previously obtained for GRB 050509b (Hjorth et al. 2005a), which occurred within a quiescent galaxy with little or no ongoing star formation, our observations of GRB 070724A, along with those of GRB 050709, place the deepest constraints on the presence of short-time-scale SN-like emission of a short GRB in a moderately star-forming host galaxy.

This can be seen in the left-hand panel of Fig. 10, where we plot the R_c magnitude of the afterglow (or the corresponding upper limit) 1 d after the GRB in a common $z = 1$ frame, adopted from Kann et al. (2008) versus the specific SFR of the host galaxy for a sample of short GRBs with known redshift estimated by Rhoads (2008). The colour scheme in Fig. 10 represents the isotropic equivalent energy E_{iso} of the event. This effectively sets a limit to short-time-scale emission from a mini-SN, as any emission in excess to the afterglow light curve would have been detected. The constraints on short-time-scale SN-like emission are deepest for GRB 050509B and GRB 070724A for quiescent and moderately star-forming galaxies, respectively.

The extended emission observed to follow the initial gamma-ray spike in many events detected by *Swift* and BATSE has also been suggested as a possible indicator of progenitor diversity within the short-GRB population. This phenomenon can generally be characterized by additional gamma-ray emission lasting several tens of seconds and fluence values that in some cases exceed that of the ini-

tial short-GRB spike. The nature of this emission has recently been discussed in detail by Perley et al. (2008) who found that roughly 30 per cent of short GRBs detected by *Swift* exhibit it in some form. They also find that the extended-to-prompt fluence ratio exhibits a large variance, with no clear correlation between the brightness or fluence of the initial spike and that of the subsequent extended emission.

We plot the ratio of the extended emission fluence to that of the initial spike (or limit thereof) adopted from Perley et al. (2008) versus the specific SFR of a subset of short GRBs with known redshift, including GRB 070724A, in the right-hand panel of Fig. 10 . There is no clear correlation between the events with significant extended emission and the type of galaxy harbouring them, although the limited sample size makes the analysis far from conclusive. Despite this, placing such constraints on additional optical and gamma-ray components of short GRBs in galaxies of varying SFRs and hence stellar populations begins to give us insights into the possible diversity of their progenitors.

Unless short GRBs are eventually found to be accompanied by tell-tale emission features like the SNe associated with long-duration GRBs, the only definitive understanding of their progenitors will come from possible associations to direct gravitational or neutrino signals. Therefore, continued attempts to observe optical components from processes not associated with the standard afterglow emission from short GRB remain vital to our understanding of the nature of these events.

Denmark, Finland, Iceland, Norway and Sweden, and with the William Herschel Telescope in the Spanish Observatorio del Roque de los Muchachos of the Instituto de Astrofísica de Canarias. We thank the VLT staff for excellent support performing the ToO observations of the host galaxy. Collection of SMARTS data is supported by NSF-AST 0707627. This work was supported in part by the U.S. Department of Energy contract to SLAC no. DE-AC3-76SF00515.

NOTE ADDED IN PRESS

The authors would like to note that Berger et al. (2009) reported the detection of a near-IR and optical afterglow associated with GRB 070724A three weeks after the submission of this paper. They report the detection of the afterglow starting 2.3 h after the burst at $K_s = 19.56 \pm 0.16$, consistent with our K-band upper limit from observations made at roughly the same time. Berger et al. note that the optical to NIR spectral index is much redder than expected from the standard afterglow model, pointing to the possibility of either significant dust exhibition along the line of sight or a non-afterglow origin to the IR emission. The former scenario would explain the lack of an optical afterglow detection and likewise significantly impact our constraints on the LP-SN model parameters, although it is not entirely supported by our late-time X-ray N_H column density estimates.

REFERENCES

Asplund M., Grevesse N., Sauval A. J., Allende Prieto C., Kiselman D., 2004, A&A, 417, 751
Barthelmy S. D. et al., 2005, Nat, 438, 994
Belczynski K., Sadowski A., Rasio F. A., Bulik T., 2006, ApJ, 650, 303
Berger E., 2006, BAAS, 38, 1171
Berger E., 2009, ApJ, 690, 231
Berger E. et al., 2005, Nat, 438, 988
Berger E. et al., 2007, ApJ, 664, 1000
Berger E., Cenko S. B., Fox D. B., Cucchiara A., 2009, ApJ, 704, 877
Berger E., Shin M.-S., Mulchaey J. S., Jeltema T. E., 2007, ApJ, 660, 496
Bertin E., Arnouts S., 1996, A&AS, 117, 393
Bloom J. S., 2007, GRB Coordinates Network, 6658
Bloom J. S., Butler N. R., 2007, GRB Coordinates Network, 6661
Bloom J. S. et al., 2006, ApJ, 638, 354
Bloom J. S. et al., 2007, ApJ, 654, 878
Bloom J. S., Kulkarni S. R., Djorgovski S. G., 2002, AJ, 123, 1111
Bloom J. S., Sigurdsson S., Pols O. R., 1999, MNRAS, 305, 763
Butler N. R., Kocevski D., 2007a, ApJ, 663, 407
Butler N. R., Kocevski D., 2007b, ApJ, 668, 400
Cardelli J. A., Clayton G. C., Mathis J. S., 1989, ApJ, 345, 245
Cenko S. B., Rau A., Berger E., Price P. A., Cucchiara A., 2007, GRB Coordinates Network, 6664
Chandra P., Frail D. A., 2007, GRB Coordinates Network, 6667
Christensen L., Hjorth J., Gorosabel J., 2004, A&A, 425, 913
Covino S. et al., 2006, A&A, 447, L5
Covino S., Piranomonte S., Vergani S. D., D'Avanzo P., Stella L., 2007, GRB Coordinates Network, 6666
Cucchiara A., Fox D. B., Cenko S. B., Berger E., Price P. A., Radomski J., 2007, GRB Coordinates Network, 6665
de Pasquale M., Ziaeepour H., 2007, GRB Coordinates Network, 6660

Dickey J. M., Lockman F. J., 1990, ARA&A, 28, 215
Eichler D., Livio M., Piran T., Schramm D. N., 1989, Nat, 340, 126
Ferrero P. et al., 2007, AJ, 134, 2118
Foley R. J. et al., 2003, PASP, 115, 1220
Fox D. B. et al., 2005, Nat, 437, 845
Freeman P. E., Kashyap V., Rosner R., Lamb D. Q., 2002, ApJS, 138, 185
Freiburghaus C., Rosswog S., Thielemann F.-K., 1999, ApJ, 525, L121
Fruchter A. S. et al., 2006, Nat, 441, 463
Fryer C. L., Woosley S. E., Hartmann D. H., 1999, ApJ, 526, 152
Galama T. J. et al., 1998, Nat, 395, 670
Gehrels N. et al., 2008, ApJ, 689, 1161
Gehrels N. et al., 2005, Nat, 437, 851
Gorosabel J. et al., 2006, A&A, 450, 87
Hjorth J. et al., 2005a, ApJ, 630, L117
Hjorth J. et al., 2005b, Nat, 437, 859
Izotov Y. I., Stasińska G., Meynet G., Guseva N. G., Thuan T. X., 2006, A&A, 448, 955
Kalberla P. M. W., Burton W. B., Hartmann D., Arnal E. M., Bajaja E., Morras R., Pöppel W. G. L., 2005, A&A, 440, 775
Kann D. A. et al., 2008, preprint (arXiv e-prints)
Kennicutt R. C., Jr., 1998, ARA&A, 36, 189
Kewley L. J., Dopita M. A., 2002, ApJS, 142, 35
Kouveliotou C., Meegan C. A., Fishman G. J., Bhat N. P., Briggs M. S., Koshut T. M., Paciesas W. S., Pendleton G. N., 1993, ApJ, 413, L101
Kulkarni S. R., 2005, preprint (arXiv e-prints)
Lee W. H., Ramirez-Ruiz E., 2007, New J. Phys., 9, 17
Lee W. H., Ramirez-Ruiz E., López-Cámara D., 2009, ApJ, 699, L93
Leitherer C. et al., 1999, ApJS, 123, 3
Li L.-X., Paczyński B., 1998, ApJ, 507, L59
Malesani D. et al., 2007, A&A, 473, 77
Modjaz M. et al., 2008, AJ, 135, 1136
Nakar E., 2007, Phys. Rep., 442, 166
Narayan R., Piran T., Shemi A., 1991, ApJ, 379, L17
Nysewander M., Fruchter A. S., Pe'er A., 2008, preprint (arXiv e-prints)
Oke J. B. et al., 1995, PASP, 107, 375
Osterbrock D. E., 1989, in Osterbrock D. E., ed., Astrophysics of Gaseous Nebulae and Active Galactic Nuclei
Paczynski B., 1986, ApJ, 308, L43
Paczynski B., 1991, Acta Astron., 41, 257
Page K. L., Ziaeepour H., 2007, GRB Coordinates Network, 6659
Parsons A. et al., 2007, GRB Coordinates Network, 6656
Perley D. A. et al., 2008, ApJ, 672, 449
Perley D. A. et al., 2009, preprint (arXiv e-prints)
Prochaska J. X. et al., 2006, ApJ, 642, 989
Rhoads J. E., 2008, preprint (arXiv e-prints)
Richmond M. W. et al., 1996, AJ, 111, 327
Rosswog S., 2007, MNRAS, 376, L48
Rosswog S., Ramirez-Ruiz E., 2002, MNRAS, 336, L7
Rosswog S., Liebendörfer M., Thielemann F.-K., Davies M. B., Benz W., Piran T., 1999, A&A, 341, 499
Sari R., Piran T., Narayan R., 1998, ApJ, 497, L17
Schlegel D. J., Finkbeiner D. P., Davis M., 1998, ApJ, 500, 525
Soderberg A. M. et al., 2006, ApJ, 650, 261
Sollerman J. et al., 2006, A&A, 454, 503
Troja E., King A. R., O'Brien P. T., Lyons N., Cusumano G., 2008, MNRAS, 385, L10
Woosley S. E., Bloom J. S., 2006, ARA&A, 44, 507
Ziaeepour H. et al., 2007, GRB Coordinates Network, 6654

This paper has been typeset from a TEX/LATEX file prepared by the author.